ANL-76-77



# PHYSICS AND PUMP COASTDOWN CALCULATIONS FOR A MODEL OF A 4000 MWe OXIDE-FUELED LMFBR

by

H. H. Hummel, Kalimullah,
and P. A. Pizzica


ARGONNE NATIONAL LABORATORY, ARGONNE, ILLINOIS

Prepared for the U. S. NUCLEAR REGULATORY COMMISSION
under Contract W-31-109-Eng-38

Printed in the United States of America
Available from
National Technical Information Service
U. S. Department of Commerce
5285 Port Royal Road
Springfield, Virginia 22161
Price: Printed Copy $4.00; Microfiche $2.25

Distribution Category:
Advanced Reactor Safety
Research—Fast Reactors
(NRC-7)

ANL-76-77

ARGONNE NATIONAL LABORATORY
9700 South Cass Avenue
Argonne, Illinois 60439

# PHYSICS AND PUMP COASTDOWN CALCULATIONS FOR A MODEL OF A 4000 MWe OXIDE-FUELED LMFBR

by

H. H. Hummel, Kalimullah,
and P. A. Pizzica

Applied Physics Division

June 1976

TABLE OF CONTENTS


| No. | Title | Page |
|---|---|---|
| ABSTRACT | | 1 |
| I. | INTRODUCTION AND SUMMARY | 1 |
| II. | PHYSICS CALCULATIONS | 1 |
| | A. Geometry | 1 |
| | B. Reactor Composition at Beginning of Life | 3 |
| | C. Calculation of Power and Reactivity Distributions | 8 |
| III. | SAS CALCULATIONS | 8 |
| | A. SAS Model of Reactor | 8 |
| | B. Loss-of-Flow Calculations with Parametric Study of Axial Expansion, Coolant Film Motion, Clad Motion, and PRIMAR-I Vs. PRIMAR-II | 8 |
| | C. Pump Coastdown Calculations Comparing PRIMAR-I and PRIMAR-II for Various Flow Reduction Rates and Doppler Coefficients | 18 |
| IV. | CONCLUSIONS | 18 |
| REFERENCES | | 21 |

## LIST OF TABLES


| No. | Title | Page |
|---|---|---|
| I. | Geometry of a Two-Zone 4000 MWe Reactor. . . . . | 2 |
| II. | Reactor Composition at Beginning of Life . . . . . | 5 |
| III. | Regionwise Distribution of Power and Reactivity Worths at BOL for the 4000 MWe LMFBR . . . . . | 9 |
| IV. | Ten Channel Model of BOL State of 4000 MWe LMFBR . . . . . | 13 |
| V. | Boiling Times for Case 2 of Table VI . . . . . | 14 |
| VI. | Conditions at Fuel Failure for 4000 MWe Pump Coastdown Calculations . . . . . | 15 |
| VII. | Inlet Plenum Pressure vs. Time for Case 2 of Table VI. . . . | 17 |
| VIII. | Summary of Results for Sodium Voiding Ramp Rates for Additional Pump Coastdown Calculations Using Flow Coastdown Rate and Doppler Coefficient as Parameters . . . . . | 19 |


## LIST OF FIGURES


| No. | Title | Page |
|---|---|---|
| 1. | R-Z Model of the Lower Half of a 4000 MWe LMFBR. All dimensions are in cm. The inner and outer cores and the axial blankets have been split into regions which correspond to SAS heat transfer modes by channel. . . . . | 4 |
| 2. | Axial Distribution of Fuel Worths for SAS Channels. Letters "A," "B," "C," etc., denote Channels 1, 2, 3, etc., respectively . . . . . | 10 |
| 3. | Axial Distribution of Sodium Void Worth for SAS Channels . . | 11 |
| 4. | Axial Distribution of Steel Worth for SAS Channels . . . . . | 12 |

# PHYSICS AND PUMP COASTDOWN CALCULATIONS FOR A MODEL OF A 4000 MWe OXIDE-FUELED LMFBR

by

H. H. Hummel, Kalimullah, and P. A. Pizzica

## ABSTRACT

Pump coastdown calculations for a model of a 4000 MWe LMFBR similar to one studied by Bleiweis et al gave sodium boiling voiding reactivity ramp rates of about $25/sec instead of up to $250/sec obtained previously. This discrepancy has not been satisfactorily explained. If hydraulic coupling among channels is neglected, as was the case in the calculations of Bleiweis et al, ramp rates up to $60/sec are found in some cases.

## I. INTRODUCTION AND SUMMARY

In order to study loss-of-flow (LOF) calculations in LMFBR's in the limiting case of a very positive sodium void effect, a model of a 4000 MWe oxide-fueled LMFBR essentially identical with one previously studied by Bleiweis et al[1] was selected. Only the beginning-of-life (BOL) state was considered. Flow was assumed to decrease according to an assumed pump coastdown curve, and LOF calculations were carried out with the SAS 3A code.[2,3] The surprising result was obtained that the maximum sodium void rate attained was only about $25/sec, although Bleiweis et al had found values up to $250/sec. A number of parameters were investigated in an attempt to understand this discrepancy, with only limited success. It was found that at rapid flow coastdown rates somewhat more rapid voiding rates were attained with the PRIMAR I module,[4] used by Bleiweis et al, than with the more advanced PRIMAR II,[5] currently used in SAS 3A calculations.

The major difference between our results and those of Bleiweis et al thus remained unexplained, as we were never able to attain a boiling voiding ramp rate greater than $60/sec, and the rates found were generally around $20/sec.

## II. PHYSICS CALCULATIONS

### A. Geometry

Starting from the core dimensions of a two-zone 4000 MWe reactor given in reference 1 and keeping the overall dimensions fixed, the dimensions shown in Table I were chosen. First, the cross-sectional area of a single hexagonal unit was selected. The equivalent radii were then found from the number of subassemblies in various zones. The inner

TABLE I. Geometry of a Two-Zone 4000 MWe Reactor

| | |
|---|---|
| Power | 4000 MWe (10,000 MWt) |
| Cross-sectional area of a single hexagonal unit | 162.25 $cm^2$ |
| Inner core region: | |
| Number of rows of subassemblies | 14 |
| Number of subassemblies | 547 |
| Equivalent radius | 168.08 cm |
| Outer core region: | |
| Number of rows of subassemblies | 5 |
| Number of subassemblies | 480 |
| Equivalent outer radius | 230.31 cm |
| Radial blanket region: | |
| Number of rows of subassemblies | 2 |
| Number of subassemblies | 234 |
| Equivalent outer radius | 255.20 cm |
| Core height | 127.0 cm |
| Axial blanket thickness | 30.5 cm each |
| Subassembly can outer width across flats | 13.561 cm |
| Subassembly lattice pitch | 13.688 cm |
| Subassembly can wall thickness | 0.330 cm |
| Fuel pins/subassembly | 217 |
| Pin clad outer diamter | 0.6138 cm |
| Clad thickness | 0.0361 cm |
| Fuel pellet outer diameter | 0.5266 cm |

and outer core zones were chosen of as equal volumes as possible with complete rows of subassemblies. Control subassemblies were not taken into account in this analysis. An R-Z model of the reactor corresponding to the SAS channel definition given in Table IV is shown in Fig. 1.

B. Reactor Composition at Beginning of Life

The volume fractions of fuel, sodium, and stainless steel in the inner core, outer core and radial blanket subassemblies were taken from reference 1. Table II describes the composition of the reactor at the beginning of the first cycle. An asterisk indicates basic input data.

Average sodium density used in the neutronics calculations was found from the average sodium temperature in the reactor. The inlet and outlet temperatures of sodium were taken from reference 1 as 400°C and 560°C; corresponding to this,the average sodium temperature was taken as 480°C.

The stainless steel was assumed to be identical to the steel used in the Clinch River Breeder Reactor (CRBR),[6] both in density and composition.

The fuel in the inner and outer core regions was taken to be a mixture $UO_2$ and $PuO_2$, and $UO_2$ in the axial and radial blanket regions. The isotopic compositions of uranium and plutonium in the core regions were assumed to be identical to those in the core regions of the CRBR, and the isotopic composition of uranium in the blanket regions identical to that in the blanket regions of the CRBR. The theoretical densities of $UO_2$ and $PuO_2$ were taken from reference 8, uranium here implying natural uranium and plutonium implying pure plutonium-239. The theoretical densities of the oxides of the different isotopes of plutonium were determined from the fact that the densities followed the same proportions to one another as the molecular weights of these pure isotope oxides. The theoretical densities of $U^{235}O_2$ and $U^{238}O_2$ were found from $U^{nat}O_2$ theoretical density using the same rule. This rule obviously implies that the theoretical atom density of $Pu^{239}$ in $Pu^{239}O_2$ is precisely equal to the atom density of $Pu^{240}$ in $Pu^{240}O_2$, and so on. This atom density of the different plutonium isotopes in their oxides is called theoretical <u>full atom density</u> of plutonium in plutonium oxide in the following text.

The smear-to-theoretical density ratios were assumed identical to those of the CRBR, thus fixing the smeared full atom densities of U in $UO_2$ and Pu in $PuO_2$ in inner and outer cores and axial and radial blankets. From these smeared full atom densities and the isotopic composition, the atom densities of the different isotopes in $UO_2$ and $PuO_2$ were found.

The volume fractions of $PuO_2$ in inner and outer cores given in Table II were determined based on the requirement that the peak power densities in the two core zones be equal, and the effective multiplication factor be 1.1 at the beginning of life (BOL) to allow for control poison, burnup and fission-products. Two dimensional (R-Z) diffusion theory in 27 groups was used for these calculations.

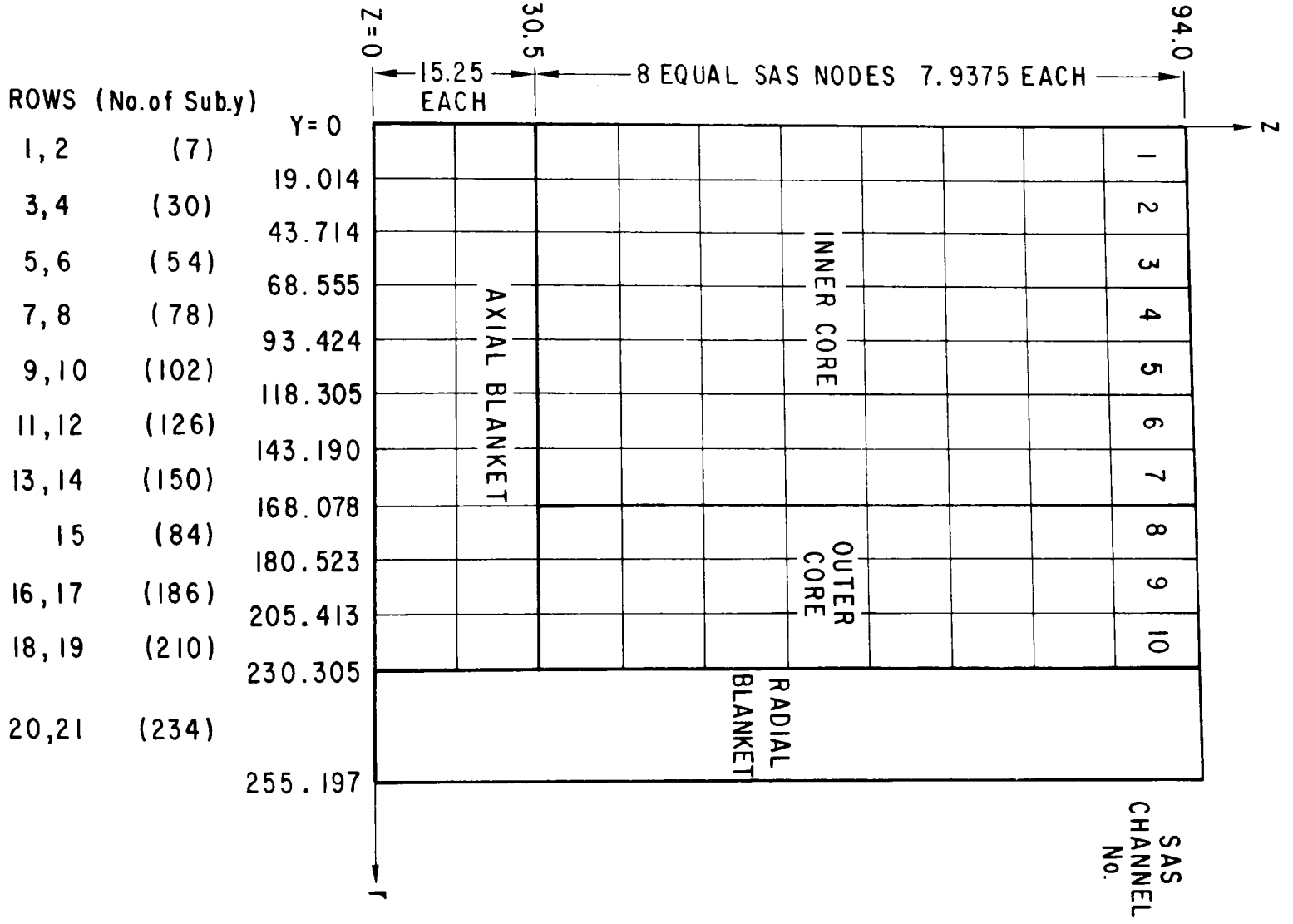


Fig. 1. R-Z Model of the Lower Half of a 4000 MWe LMFBR. All dimensions are in cm. The inner and outer cores and the axial blankets have been split into regions which correspond to SAS heat transfer nodes by channel.

TABLE II. Reactor Composition at Beginning of Life

| | |
|---|---|
| *Inner and outer core volume fractions: | |
| Fuel | 0.308 |
| Sodium | 0.511 |
| Stainless steel | 0.181 |
| *Radial blanket volume fractions: | |
| Fuel | 0.565 |
| Sodium | 0.295 |
| Stainless steel | 0.140 |
| *Average sodium temperature | 480°C |
| Average sodium density | 0.835 $gm/cm^3$ |
| *Composition of steel by weight: | |
| Iron | 64.75 w/o |
| Chromium | 17.50 w/o |
| Nickel | 13.50 w/o |
| Molybdenum | 2.50 w/o |
| Manganese | 1.75 w/o |
| *Density of steel | 7.94 $gm/cm^3$ |
| *Fuel in inner and outer cores | $UO_2$-$PuO_2$ mixture |
| *Fuel in axial and radial blanets | $UO_2$ |
| *Isotopic composition of Pu by number of atoms: | |
| $^{239}Pu$:$^{240}Pu$:$^{241}Pu$:$^{242}Pu$ | 68.11:19.35 :10.14:2.40 a/o |
| *Isotopic composition of U in inner and outer cores by number of atoms: | |
| $^{235}U$:$^{238}U$ | 0.697:99.303 a/o |
| *Isotopic composition of U in axial and radial blankets by number of atoms: | |
| $^{235}U$:$^{238}U$ | 0.220:99.780 a/o |

TABLE II. (cont'd)

| | |
|---|---|
| **Average atomic weights:** | |
| Plutonium in inner and outer cores | 239.60 |
| Uranium in inner and outer cores | 238.10 |
| Uranium in axial and radial blankets | 238.12 |
| **Theoretical densities:** | |
| *$U^{nat}O_2$ (0.715 a/o $^{235}U$) | 10.96 gm/cm$^3$ |
| *$^{239}PuO_2$ | 11.46 gm/cm$^3$ |
| $^{238}UO_2$ | 10.9609 gm/cm$^3$ |
| $UO_2$ in inner and outer cores | 10.9600 gm/cm$^3$ |
| $PuO_2$ in inner and outer cores | 11.4799 gm/cm$^3$ |
| $UO_2$ in axial and radial blankets | 10.9606 gm/cm$^3$ |
| Avogadro's number | 0.60247 atoms/gm-mole[a] |
| **Theoretical full atom densities:** | |
| Pu in $PuO_2$ | 0.02547 atoms/cm$^3$ |
| U in $UO_2$ | 0.02445 atoms/cm$^3$ |
| ***Smear-to-theoretical density ratio of fuels:** | |
| Radial blanket | 0.9366 |
| Inner and outer cores and axial blankets | 0.8550 |
| **Atom densities of smeared $UO_2$ fueling radial blanket:** | |
| $^{235}U$ | 0.5033 x 10$^{-4}$ atoms/cm$^3$ $UO_2$ |
| $^{238}U$ | 0.02285 atoms/cm$^3$ $UO_2$ |
| O | 0.04579 atoms/cm$^3$ $UO_2$ |
| **Atom densities of smeared $UO_2$ fueling axial blankets:** | |
| $^{235}U$ | 0.4594 x 10$^{-4}$ atoms/cm$^3$ $UO_2$ |
| $^{238}U$ | 0.02085 atoms/cm$^3$ $UO_2$ |
| O | 0.04180 atoms/cm$^3$ $UO_2$ |

[a] A factor of $10^{24}$ has been omitted in all atom concentrations.

TABLE II. (cont'd)

| | |
|---|---|
| **Atom Densities of smeared $UO_2$ fueling inner and outer cores:** | |
| $^{235}U$ | $1.457 \times 10^{-4}$ atoms/cm$^3$ $UO_2$ |
| $^{238}U$ | 0.02076 atoms/cm$^3$ $UO_2$ |
| O | 0.04180 atoms/cm$^3$ $UO_2$ |
| **Atoms densities of smeared $PuO_2$ fueling inner and outer cores:** | |
| $^{239}Pu$ | 0.01483 atoms/cm$^3$ $PuO_2$ |
| $^{240}Pu$ | 0.00421 atoms/cm$^3$ $PuO_2$ |
| $^{241}Pu$ | 0.00221 atoms/cm$^3$ $PuO_2$ |
| $^{242}Pu$ | $0.522 \times 10^{-3}$ atoms/cm$^3$ $PuO_2$ |
| O | 0.04354 atoms/cm$^3$ $PuO_2$ |
| **Inner core fuel composition and density:** | |
| *$PuO_2$ volume fraction | 0.04832 |
| $UO_2$ volume fraction | 0.25968 |
| Enrichment, Pu/(U + Pu) | 16.234 a/o |
| Mixed oxide density | 9.440 gm/cm$^3$ smeared |
| **Outer core fuel composition and density:** | |
| *$PuO_2$ volume fraction | 0.05807 |
| $UO_2$ volume fraction | 0.24993 |
| Enrichment, Pu/(U + Pu) | 19.488 a/o |
| Mixed oxide density | 9.454 gm/cm$^3$ smeared |
| Radial blanket $UO_2$ density | 10.266 gm/cm$^3$ smeared |
| Axial blanket $UO_2$ density | 9.371 gm/cm$^3$ smeared |

C. Calculation of Power and Reactivity Distributions

The power and the reactivity worths of sodium, steel and fuel, and the unvoided and voided Doppler coefficients were calculated based on diffusion[9] and first-order perturbation[10] theories using the R-Z model of the reactor shown in Fig. 1. Two sets of 27-group real and adjoint fluxes at a uniform fuel temperature of 1100°K, one set with the normal amount of sodium and the other with the volume fraction of sodium reduced in the core and axial blanket regions to 0.0727 from 0.511, were generated for using in perturbation calculations. The volume fraction 0.0727 was assumed to represent the sodium contained outside the subassembly cans whose thermohydraulic behavior is not analysed by the SAS Code and which is assumed to be always present even after the sodium inside the cans has voided. (Based on the subassembly dimensions given in Table I, this volume fraction should have been 0.0184, thus lowering the voided Doppler coefficient by about 10%. The effect of such reductions is parametrically studied and discussed in the next section.) The power distribution given in Table III is based on the unvoided real flux. The unvoided Doppler coefficient and the sodium void reactivity distributions were calculated using the first set of fluxes (with normal sodium) for the unperturbed reactor, and the distributions of the voided Doppler coefficient, steel and fuel worths were calculated using the second set of fluxes because extensive sodium voiding was believed to occur before any appreciable clad and fuel motion. The Doppler coefficients were calculated over the temperature range 1100°K-2200°K. With the help of a processing program the distributions of power and reactivity worths were put in the form required by the SAS Code. The totals by region are summarized in Table III. Axial distributions of fuel, sodium, and steel worths for the SAS channels are given in Fig. 2, 3, and 4 respectively. In these figures channels 1, 2, 3 etc. are denoted by "A", "B", "C" etc.

## III. SAS CALCULATIONS

A. SAS Model of Reactor

Subassembly rings were grouped into channels for the SAS 3A code as indicated in Table IV. The radial blanket was ignored in the SAS calculations.

B. Loss-of-Flow Calculations with Parametric Study of Axial Expansion, Coolant Film Motion, Clad Motion, and PRIMAR-I vs. PRIMAR-II

Boiling times for one of these cases are given in Table V, and conditions at the time of fuel failure are given in Table VI. The calculations were not carried to complete disassembly because of the failure of SAS modeling. As seen in Table VI, there was still a considerable amount of liquid sodium in the core at the time of fuel failure. One difficulty that arose from this was that, at the time these calculations were run, it was possible to trigger fuel slumping with the SLUMPY module at axial pin nodes in which sodium was still present, although the SLUMPY modeling assumes sodium to be absent. A result of this was that, when slumping was triggered at

TABLE III. Regionwise Distribution of Power and Reactivity Worths at BOL for the 4000 MWe LMFBR

| Power or Reactivity | Inner Core | Outer Core | Axial Blankets | Radial Blanket | Total |
|---|---|---|---|---|---|
| Power, MWt | 5944.8 | 3920.5 | 79.8 | 54.9 | 10000 |
| Sodium void $\frac{\Delta k}{k} \times 10^3$ | 20.94 | 1.62 | -4.86 | -0.52 | 17.18 |
| Unvoided Doppler coefficient $T \frac{dk}{kdt} \times 10^3$ | -6.833 | -2.388 | -0.367 | -0.0947 | -9.684 |
| Voided[a] Doppler coefficient $T \frac{dk}{kdt} \times 10^3$ | -3.776 | -1.157 | -0.226 | -0.0865 | -5.245 |
| Steel worth $\frac{\Delta k}{k} \times 10^3$ | -49.71 | -9.07 | 9.77 | 1.38 | -47.62 |
| Fuel worth $\frac{\Delta k}{k} \times 10^3$ | 214.90 | 122.49 | 21.20 | 24.62 | 383.22 |

[a]The sodium outside the subassembly cans is assumed to be still present. A volume fraction of 0.0727 of the reactor was assumed for this sodium. The radial blanket subassemblies were not voided.

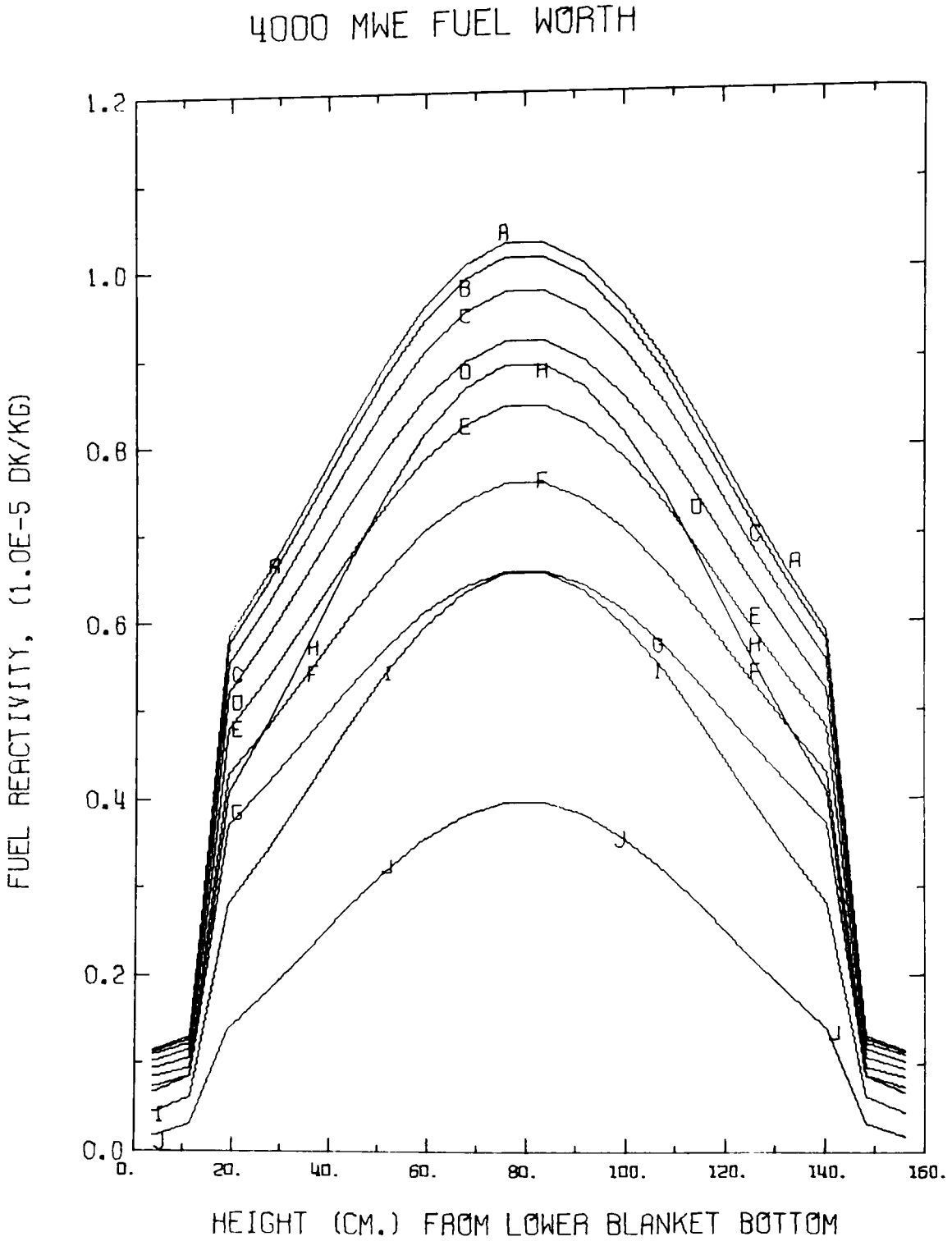


Fig. 2. Axial Distribution of Fuel Worths for SAS Channels. Letters "A," "B," "C," etc., denote Channels 1, 2, 3, etc., respectively.

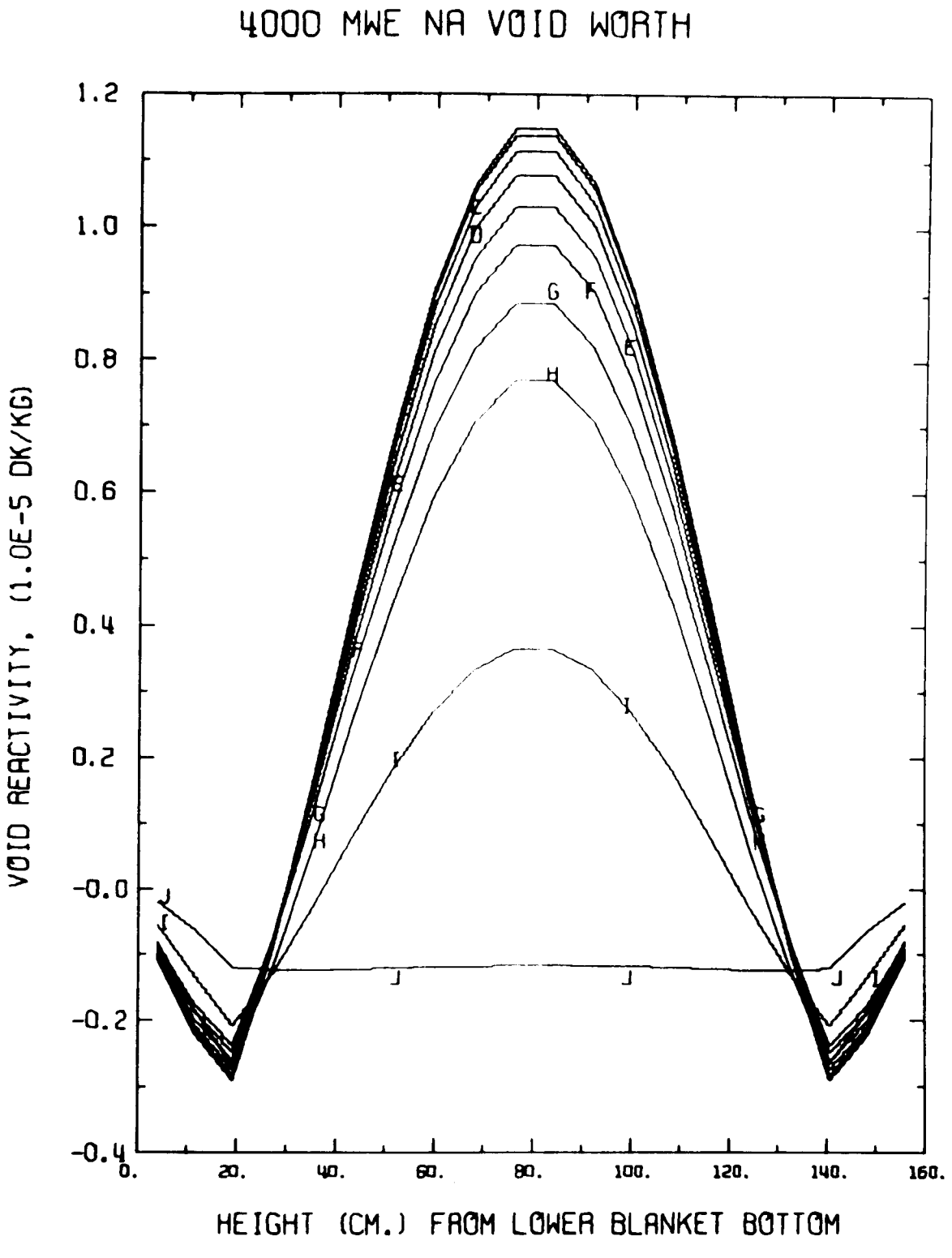


Fig. 3. Axial Distribution of Sodium Void Worth for SAS Channels.

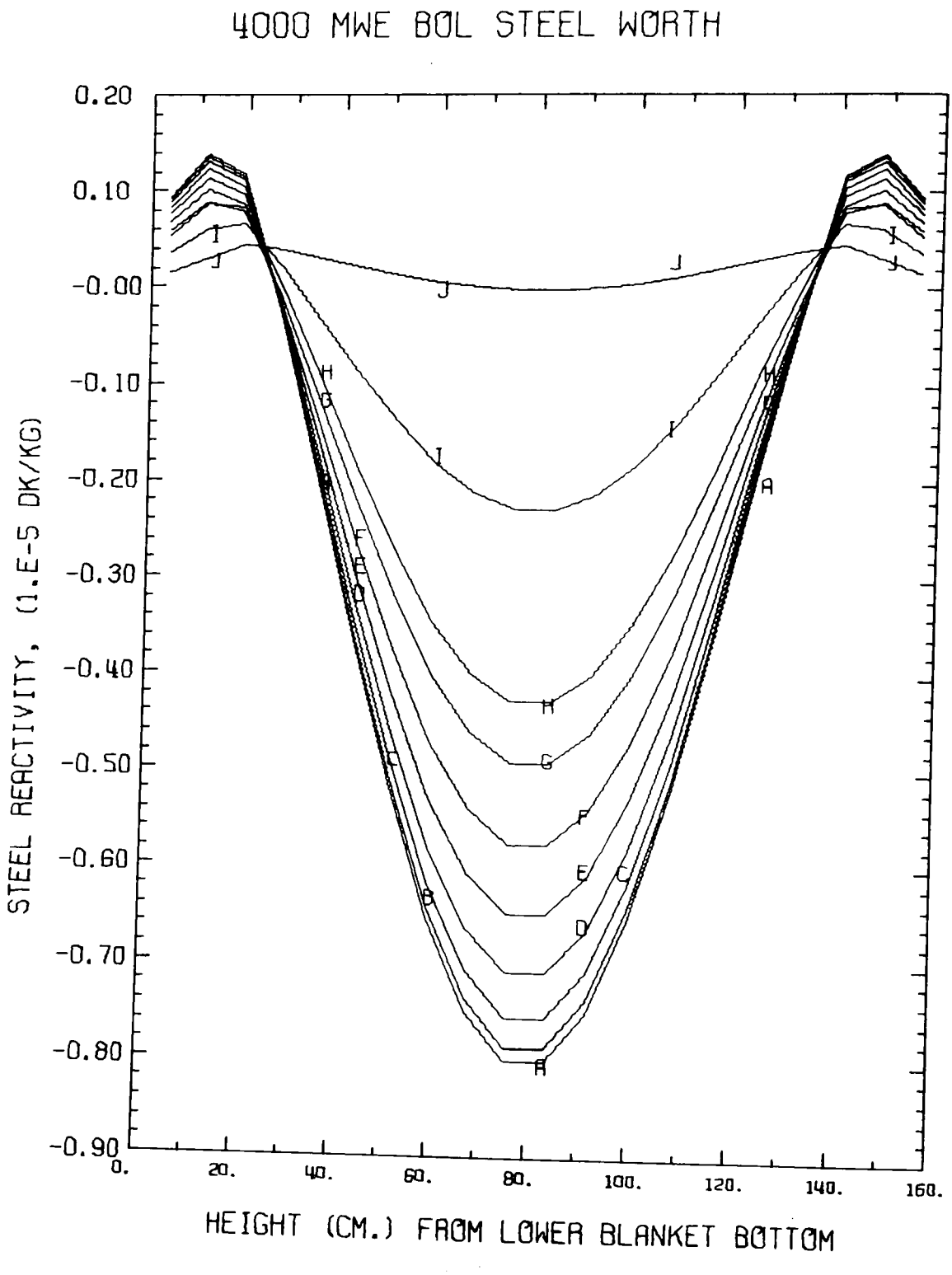


Fig. 4. Axial Distribution of Steel Worth for SAS Channels.

TABLE IV. Ten Channel Model of BOL State of 4000 MWe LMFBR

| SAS Channel | Number of Subassemblies (Ring) | Relative Radial Power | Coolant[(a)] Mass Velocity, $g/cm^2$-sec |
|---|---|---|---|
| 1 | 7(1,2) | 1.000 | 725.2 |
| 2 | 30(3,4) | 0.9955 | 721.9 |
| 3 | 54(5,6) | 0.9653 | 714.5 |
| 4 | 78(7,8) | 0.9694 | 703.0 |
| 5 | 102(9,10) | 0.9480 | 687.5 |
| 6 | 126(11,12) | 0.9204 | 667.5 |
| 7 | 150(13,14) | 0.8811 | 639.0 |
| 8 | 84(15) | 0.9642 | 699.2 |
| 9 | 186(16,17) | 0.8128 | 589.4 |
| 10 | 210(18,19) | 0.4962 | 359.8 |
| Total | 1027 | | |

[(a)] Power to flow ratio equal for all channels.

TABLE V. Boiling Times for Case 2 of Table VI

| Channel | Boiling Time, Sec. | Normalized[a] Power at Boiling Initiation |
|---|---|---|
| 1 | 13.996 | 1.060 |
| 2 | 14.010 | 1.060 |
| 3 | 14.040 | 1.060 |
| 4 | 14.092 | 1.061 |
| 5 | 14.184 | 1.056 |
| 6 | 14.340 | 1.048 |
| 7 | 15.237 | 42.8 |
| 8 | - | - |
| 9 | 15.267 | 31.4 |
| 10 | - | - |

[a]Relative to steady-state power.

TABLE VI. Conditions at Fuel Failure for 4000 MWe Pump Coastdown Calculations

| Case | 1 | | 2 | | 3 | | 4 |
|---|---|---|---|---|---|---|---|
| PRIMAR | New | | New | | New | | Old |
| Coolant Film | Movable | | Static | | Static | | Static |
| Axial Exp. Feedback | No | | No | | Yes | | No |
| Assumed Fuel Melt Fraction at Failure | Low | High | Low | High | Low | High | Low |
| Time, Sec | 15.604 | 15.616 | 15.214 | 15.254 | 18.827 | 18.990 | 10.050 |
| Power | 63 | 175 | 41 | 159 | 12.8 | 49 | 178 |
| Reactivity, $ | | | | | | | |
| Na Void | 2.03 | 2.34 | 2.04 | 2.54 | 3.17 | 3.62 | 2.09 |
| Doppler | -1.05 | -1.25 | -1.06 | -1.54 | -0.95 | -1.21 | -1.07 |
| Clad Motion | - | - | - | - | - | 0.49 | - |
| Axial Exp. | - | - | - | - | -1.36 | -1.88 | - |
| Net | 0.977 | 1.000 | 0.954 | 1.000 | 0.864 | 0.959 | 1.018 |
| Reactivity Ramp Rate, $/Sec | | | | | | | |
| Na Void | 13 | 17 | 9 | 13 | 12 | 11 | 28 |
| Clad Motion | - | - | - | - | - | 9 | - |
| Max. Fuel Temp, °C (unfailed pin) | 3300 | 4000 | 3300 | 4230 | 3000 | 4100 | 3240 |

| Channel | Fraction Core Voided | Max. Fuel Melt Fraction | Fraction Core Voided | Max. Fuel Melt Fraction | Fraction Core Voided | Max. Fuel Melt Fraction | Fraction Core Voided | Max. Fuel Melt Fraction | Fraction Core Voided | Max. Fuel Melt Fraction | Fraction Core Voided | Max. Fuel Melt Fraction | Fraction Core Voided | Max. Fuel Melt Fraction |
|---|---|---|---|---|---|---|---|---|---|---|---|---|---|---|
| 1 | 0.821 | 0.528 | 0.837 | 0.895 | 0.874 | 0.529 | 0.907 | 0.906 | 0.679 | 0.437 | 0.880 | 0.812 | 0.636 | 0.400 |
| 2 | 0.628 | 0.518 | 0.677 | 0.869 | 0.854 | 0.519 | 1.000 | 0.897 | 0.821 | 0.439 | 0.753 | 0.859 | 0.615 | 0.395 |
| 3 | 0.558 | 0.501 | 0.575 | 0.858 | 0.549 | 0.521 | 0.541 | 0.891 | 0.851 | 0.414 | 0.726 | 0.776 | 0.542 | 0.379 |
| 4 | 0.370 | 0.510 | 0.426 | 0.788 | 0.592 | 0.513 | 0.741 | 0.856 | 0.747 | 0.349 | 0.704 | 0.772 | 0.465 | 0.359 |
| 5 | 0.0 | 0.509 | 0.0 | 0.751 | 0.0 | 0.506 | 0.0 | 0.821 | 0.0 | 0.302 | 0.394 | 0.734 | 0.308 | 0.326 |
| 6 | 0.0 | 0.503 | 0.0 | 0.706 | 0.0 | 0.515 | 0.0 | 0.797 | 0.0 | 0.256 | 0.224 | 0.707 | 0.150 | 0.285 |
| 7 | 0.0 | 0.441 | 0.0 | 0.668 | 0.0 | 0.518 | 0.0 | 0.775 | 0.0 | 0.193 | 0.137 | 0.675 | 0.051 | 0.220 |
| 8 | 0.581 | 0.512 | 0.622 | 0.797 | 0.0 | 0.500 | 0.0 | 0.839 | 0.722 | 0.347 | 0.713 | 0.771 | 0.423 | 0.355 |
| 9 | 0.0 | 0.352 | 0.0 | 0.601 | 0.0 | 0.515 | 0.0 | 0.691 | 0.0 | 0.094 | 0.098 | 0.616 | 0.0 | 0.115 |
| 10 | 0.0 | 0.0 | 0.0 | 0.001 | 0.0 | 0.0 | 0.0 | 0.024 | 0.0 | 0.0 | 0.0 | 0.004 | 0.0 | 0.0 |

such a node, the Doppler coefficient for this node was abruptly switched from the non-voided to the voided value, creating a spurious jump in reactivity that amounted to \$0.10 - \$0.30 altogether and sending k far above prompt critical. A fix was later put into the code that suppressed slumping at nodes where liquid sodium was still present. A problem in the code harder to correct is the inadequacy of the fuel-coolant interaction modeling for the situation of fuel failure in a LOF accident with liquid sodium still present. Because of this shortcoming in the code the present investigation was limited to determination of sodium voiding rates prior to fuel failure, with fuel failure conditions treated parametrically.

The most interesting result from these studies is that the very high sodium voiding ramp rates (up to \$250/sec) reported in Ref. 1 were not obtained; ramp rates at incipient fuel failure conditions are under \$20/sec, averaged over the previous 20 to 30 milliseconds. Bleiweis[11] suggested that the reason for the difference is the use in his case of the original version of the SAS PRIMAR module, PRIMAR-I, for primary-coolant loop calculations, while we have used the advanced version, PRIMAR-II. In the original version of PRIMAR the inlet coolant plenum pressure is determined as the specified outlet plenum pressure plus the pump head. In the advanced PRIMAR the inlet coolant plenum pressure is determined by a pressure drop calculation around the primary loop, the outlet plenum pressure again being fixed. Expulsion of the lower liquid slug causes a buildup of pressure in the inlet plenum to 4-5 atm as is shown in Table VII for Case 2 in Table VI, slowing down further ejection. With the original PRIMAR the inlet plenum pressure, which has typically fallen to about 2 atm as a result of the pump head decay assumed in the LOF accident, remains fixed during the expulsion. There is thus a potentially autocatalytic situation opposed only by the Doppler effect (and by axial fuel expansion, if this is assumed present). We have run a case with the old PRIMAR to try to reproduce Bleiweis' results (Case 4 in Table VI). The sodium voiding ramp rate is higher than with the advanced PRIMAR, and reached \$40/sec over several milliseconds; the value in the table of \$28/sec is averaged over 16 milliseconds.

The effect of varying several parameters is also shown in Table VI. Increasing the fuel melt fraction required for failure tends to slightly increase the sodium voiding ramp rate. Cases 1 and 2 compare the use of the movable and static coolant film option of SAS; as found previously the final results are not much different. Cases 2 and 3 show the effect of including axial expansion feedback. This lengthens the time scale of events and eventually allows time for some clad motion to occur. Otherwise the more rapid power rise associated with more positive sodium voiding prevents clad motion from taking place. It would presumably also make fuel motion more likely, although a significant positive reactivity addition from this source in a large reactor seems to be a remote possibility. The SAS axial expansion algorithm is now known to overpredict this feedback effect by approximately a factor of 3. Even so, the net effect of axial expansion is not very important. Clad motion might not occur at all in the present model with a more correct treatment of axial expansion. On the other hand, a better treatment of incoherence effects in sodium voiding might reduce the rate of power rise, increasing the possibility of clad motion.

TABLE VII. Inlet Plenum Pressure vs. Time for Case 2 of Table VI.

| Time, sec | Inlet Plenum Pressure, atm. | Normalized[a] Power |
|---|---|---|
| 0.0 | 9.33 | 1.00 |
| 3.00 | 5.27 | 1.03 |
| 6.00 | 3.18 | 1.04 |
| 9.00 | 3.14 | 1.04 |
| 12.00 | 2.83 | 1.05 |
| 14.00 | 2.70 | 1.06 |
| 14.77 | 3.04 | 1.27 |
| 14.79 | 2.99 | 1.34 |
| 15.100 | 3.25 | 3.21 |
| 15.209 | 3.77 | 3.77 |
| 15.250 | 4.14 | 8.73 |
| 15.255 | 4.96 | 159 |
| 15.269 | 6.15 | 36.4 |

[a]Relative to steady-state power.

The flow coastdown rates for the cases in Table VI are the same as those for the third and eighth cases in Table VIII for PRIMAR-II and PRIMAR-I respectively. The effect of varying flow reduction rate on boiling voiding ramp rate is discussed in the following section.

### C. Pump Coastdown Calculations Comparing PRIMAR-I and PRIMAR-II for Various Flow Reduction Rates and Doppler Coefficients

Further studies were carried out on voiding rates in the 4000 MWe LMFBR model to try to better quantify differences between use of the old and new PRIMAR. Doppler coefficient and flow coastdown rate were used as parameters in these studies. Results are given in Table VIII. In this table the "orginal" Doppler coefficients are the ones we calculated for this model. The reduced ones are less than the original ones by 10% for sodium in and by 20% for sodium voided, which is about what was used in Ref. 1. The "reduced-20%" values are reduced another 20% beyond this. The motivation in reducing the Doppler coefficient is to see if autocatalytic tendencies develop in sodium voiding. The results show no consistent trend of sodium voiding ramp rate with Doppler coefficient in the range studied.

Fuel slumping was suppressed up to a maximum fuel temperature of 4500°C and the calculation was terminated at this point because fuel-melt fractions were about 90%, and it was felt that the calculation would not be physically meaningful at higher fuel energies. There was some tendency for ramp rate to increase with fuel energy, but maximum values were still far below the \$250/sec observed previously.[1]

The approximate flow decay period is defined as the exponential period that would produce the observed fractional flow decay. Because the decay was not really exponential this number has somewhat limited significance. In Table VIII values of this period are given based on the fractional flow decay obtained at 9.0 sec after start of the flow reduction and also at 12.0 sec. Actual fractional flow decays obtained at various times using the indicated pump head decay coefficients are also given in Table VIII. These fractional decays are given until the time boiling started.

There does not seem to be any consistent dependence of sodium voiding ramp rate on flow decay rate for PRIMAR-II. For PRIMAR-I there seems to be a trend toward higher ramp rates at higher flow decay rates. Although there does not seem to be much difference between voiding ramp rates with PRIMAR-I and PRIMAR-II at lower flow decay rates, at more rapid flow decay these ramp rates are consistently larger for PRIMAR-I, as had been expected. The one case run with SAS-2A, which had a voiding model believed to be same as that used in Ref. 1, gave results comparable to and even slightly lower than those obtained with SAS-3A at a similar flow coastdown rate.

## IV. CONCLUSIONS

The buildup of inlet plenum pressure as calculated by PRIMAR-II does seem to have some damping effect on boiling voiding ramp rates, although the effect is small compared to the discrepancy between our results and those

TABLE VIII. Summary of Results for Sodium Voiding Ramp Rates for Additional Pump Coastdown Calculations Using Flow Coastdown Rate and Doppler Coefficient as Parameters

| PRIMAR | Approx. Flow Decay Period, Sec. Based on Decay at 9.0 sec / 12.0 sec | | PDEC[a] | PDEC1[a] | PDEC2[a] | Doppler Coefficients | Range of Ramp Rates, $/sec | Average Ramp Rate, $/sec | Fractional Flow Decay at 3.0 sec | 6.0 sec | 9.0 sec | 12.0 sec | 15.0 sec |
|---|---|---|---|---|---|---|---|---|---|---|---|---|---|
| II | 6.5 | | 0.380 | $-6.43\times10^{-3}$ | $8.23\times10^{-4}$ | Original | 10-36 | 22 | 0.656 | 0.406 | 0.250 | --- | --- |
| | | | | | | Reduced-20% | 12-29 | 18 | | | | | |
| II | 8.3 | | 0.280 | $-6.43\times10^{-3}$ | $8.23\times10^{-4}$ | Original | 14-25 | 20 | 0.721 | 0.507 | 0.338 | --- | --- |
| | | | | | | Reduced | 14-23 | 21 | | | | | |
| | | | | | | Reduced-20% | 18-26 | 20 | | | | | |
| II | 8.9 | 10.2 | 0.3108 | $-1.6563\times10^{-2}$ | $3.426\times10^{-4}$ | Original | 9-24 | 13 | 0.650 | 0.466 | 0.364 | 0.304 | --- |
| II | 11.0 | 10.1 | 0.200 | $-6.43\times10^{-3}$ | $8.23\times10^{-4}$ | Original | 13-31 | 21 | 0.795 | 0.605 | 0.442 | 0.303 | --- |
| | | | | | | Reduced | 16-26 | 19 | | | | | |
| | | | | | | Reduced-20% | 16-25 | 15 | | | | | |
| I | 6.4 | | 0.240 | $-6.43\times10^{-3}$ | $8.23\times10^{-4}$ | Original | 27-57 | 40 | 0.683 | 0.449 | 0.247 | --- | --- |
| | | | | | | Reduced | 31-62 | 39 | | | | | |
| | | | | | | Reduced-20% | 26-50 | 41 | | | | | |
| I | 6.9 | | 0.35393 | $-1.6563\times10^{-2}$ | $3.426\times10^{-4}$ | Reduced-20% | 21-53 | 32 | 0.596 | 0.390 | 0.273 | --- | --- |
| I | 10.8 | 8.2 | | | | Original | 28-60 | 42 | 0.783 | 0.621 | 0.436 | 0.230 | --- |
| | | | | | | Reduced-20% | 27-52 | 38 | | | | | |
| I[b] | 8.1 | 9.3 | 0.35393 | $-1.6563\times10^{-2}$ | $3.426\times10^{-4}$ | Original | 17-29 | 22 | 0.618 | 0.432 | 0.333 | 0.276 | 0.239 |
| I | 8.9 | 10.2 | | | | Original | 18-32 | 24 | 0.650 | 0.466 | 0.364 | 0.304 | --- |
| | | | | | | Reduced | 24-41 | 31 | | | | | |
| | | | | | | Reduced-20% | 19-42 | 31 | | | | | |

[a] Coefficients in pump head decay equation $\Delta P/\Delta P_o = \exp\left[-PDEC*t - PDEC1*t^2 - PDEC2*t^3\right]$

[b] SAS 2A was used in this calculation. All others used SAS 3A.

in Ref. 1. This discrepancy thus remains unexplained. Buildup of inlet plenum pressure appears to be an important enough phenomenon to deserve a more careful calculation than is possible with the still rather crude model of PRIMAR-II. A primary loop module which explicitly models pump characteristics, has the correct number of loops, and is otherwise more accurate and detailed is needed for this purpose.

Boiling voiding ramp rates calculated here are not large enough to cause a violent disassembly. Because of the very positive sodium void coefficient, however, high ramp rates from ejection of sodium when low power pins fail remain a possibility to be investigated when better SAS modeling is available.

Although the size of this model was selected to be large enough to represent a limiting case, because of the low fuel volume fraction and density the sodium void effect for this reactor may not be outside the range for some target plant designs of interest for the foreseeable future.

Clad motion reactivity effects do not seem likely to be important in a large LMFBR because the more rapid power rise associated with a more positive sodium void effect does not allow time for much clad motion to occur.

## REFERENCES


1. P. B. Bleiweis et al, *A Comparison Study and Analysis of Models for 1000 MWe and 4000 MWe LMFBR Hypothetical Accidents,* Proc. Fast Reactor Safety Meeting, Beverly Hills, Calif., April 2-4, 1974, CONF-74041, p. 1322.

2. M. G. Stevenson et al, *Current Status and Experimental Basis of the SAS LMFBR Accident Analysis Code,* Proc. Fast Reactor Safety Meeting, Beverly Hills, Calif., April 2-4, 1974, CONF-74041, p. 1303.

3. F. E. Dunn et al, *The SAS3A LMFBR Accident Analysis Code,* ANL/RAS-75-17, Internal Memo, Reactor Analysis and Safety Division, Argonne National Laboratory, (April 1975).

4. F. E. Dunn et al, *The SAS2A LMFBR Accident Analysis Computer Code,* Argonne National Laboratory Report, ANL-8138 (October 1974).

5. F. E. Dunn, J. Travis and L. L. Smith, *The PRIMAR-II Primary Loop Hydraulic Routine in the SAS3A Code,* Argonne National Laboratory Report, to be issued.

6. *Clinch River Breeder Reactor,* Preliminary Safety Analysis Report, Project Management Corp., Oak Ridge, Tenn.

7. Kalimullah, *Calculation of Reactivity Due to Axial Expansion in a Nuclear Reactor, Quarterly Report July-September, 1975,* Physics of Reactor Safety, Argonne National Laboratory Report ANL-76-6, p.8.

8. S. McLain and J. H. Martens, Editors, *Reactor Handbook, Volume IV, Engineering,* Interscience Publishers, New York (1964) p. 177.

9. T. A. Daly et al, *The ARC System Two-Dimensional Diffusion Theory Capability, DARC2D,* Argonne National Laboratory Report, ANL-7716, (May 1972).

10. T. A. Daly et al, *The ARC System Two-Dimensional Adjunct Calculations,* Argonne National Laboratory Report, ANL-7720 (October 1972).

11. P. Bleiweis (private communication).